1964

Interferometric study of electron density in a two-dimensional plasma shock layer.

Elliott, Charles Paul.

Stanford University

INTERFEROMETRIC STUDY OF ELECTRON DENSITY IN A TWO-DIMENSIONAL PLASMA SHOCK LAYER

A THESIS
SUBMITTED TO THE DEPARTMENT OF AERONAUTICS AND ASTRONAUTICS
AND THE COMMITTEE ON THE GRADUATE DIVISION
OF STANFORD UNIVERSITY
IN PARTIAL FULFILLMENT OF THE REQUIREMENTS
FOR THE DEGREE OF
ENGINEER

By
Charles Paul Elliott
August 1964

ACKNOWLEDGMENTS

The author is indebted to Dr. Daniel Bershader for his continuing advice and encouragement, to Messrs. P. Oettinger and K. Horn for invaluable assistance in the experimental work, and to the Lockheed Missiles and Space Company for equipment and assistance.

TABLE OF CONTENTS

		page
	NOTATION	vi
I.	INTRODUCTION	1
II.	EQUILIBRIUM FLOW THEORY	
	A. Introduction	3
	B. Gas Properties Across Shock Waves	3
	C. Stagnation Line Gas Properties	7
III.	APPLICATION OF INTERFEROMETRY TO ELECTRON DENSITY MEASUREMENT	
	A. The Mach-Zehnder Interferometer	9
	B. Development of Fringe Shift Equations	10
IV.	DESCRIPTION OF EXPERIMENT	14
V.	DISCUSSION OF RESULTS	16
VI.	CONCLUSIONS	21
	REFERENCES	22

LIST OF TABLES AND ILLUSTRATIONS

Page

Table I CALCULATED STATE PROPERTIES OF EQUILIBRIUM ARGON. . . . 23

Table II SUMMARY OF TEST OBSERVATIONS. 24

Figure 1. Schematic Diagram of Shock-Generated Flow 25

2a. Flow Interferogram (M_s=11.45). 26

2b. Flow Interferogram (M_s=11.8) 26

3a. Flow Interferogram (M_s=12.0) 27

3b. Flow Interferogram (M_s=12.8) 27

4. Fringe Shifts 28

5. Density Ratio 29

6. Electron Density. 30

7. Degree of Ionization. 31

8. Stanford Shock Tube 32

9. Schematic of Optics 33

10. Blast Shutter Interferogram 34

NOTATION

English Letters

A	Angstrom unit
a	equilibrium speed of sound
B_A	partition function of argon atom
B_{A^+}	partition function of argon ion
c	speed of light
D	diameter of cylindrical leading edge of model (1/2 inch)
e_i	specific ionization energy
e_t	internal energy per unit mass due to translation
h	specific enthalpy
h_P	Planck's constant
K_λ	Gladstone-Dale constant
k	Boltzmann's constant
L	test section width
M	Mach number
M_s	incident shock Mach number
m_A	mass of argon atom
m_{A^+}	mass of argon ion
m_e	mass of electron
N_A	number density of atoms
N_{A^+}	number density of ions
N_e	number density of electrons

n	index of refraction
$n-1$	refractivity
p	pressure
q	electronic charge
R	gas constant per unit mass
$\overline{R}$	average R for the mixture
R^*	gas constant per mole
S	fringe shift; also fringe shift at $\lambda = 4500A$
S'	fringe shift at $\lambda' = 4030A$
T	temperature
v	fluid velocity relative to the standing shock (lab)
W	atomic weight of argon atom
$\overline{W}$	average atomic weight of the mixture
x	degree of ionization

Greek Letters

α	polarizability
γ	ratio of specific heats
$\Delta( )$	change in ( )
δ	shock stand-off distance
θ	argon ionization temperature
λ	observing wave length; also $\lambda = 4500A$
λ'	4030A
μ	reduced mass of ion-electron pair

ρ	mass density
$\bar{\rho}$	mean density from region 3 to stagnation line
χ	argon ionization potential
ω	frequency of observing light, corresponding to λ
ω_p	plasma frequency

Subscripts

1	region 1, initial downstream conditions
2	region 2, conditions entering the standing shock
3	region 3, conditions downstream of the standing shock
s	stagnation line conditions
A	atoms
A^+	ions
e	electrons

I. INTRODUCTION

Treatment of high temperature shock layer flows has been of interest from the point of view of hypersonic and re-entry heat transfer. Fay and Riddell [1]*) developed a correlation formula for convective stagnation point heat transfer rate in a dissociating diatomic gas, in conjunction with an experimental study by Rose and Stark [2]. Several investigators have applied a modification of this formula to stagnation point heat transfer in partially ionized argon. Reilly [3], operating in a regime where radiative heat transfer was considered negligible, measured convective heat transfer rates slightly higher than predicted by the Fay-Riddell equation applied to an ideal gas. Rutowski [4] also determined that convective heat transfer was only moderately increased by real gas effects in the partially ionized argon. Rutowski and Bershader [5] found that, for a shock Mach number of twelve, radiative and convective heat transfer rates were about equal, while the convective rate alone agreed with the Fay-Riddell ideal gas calculation. They were also able to correlate the measured radiative heat transfer to the calculated electron density, using the Kramers classical theory to relate radiation to the square of electron density.

The importance of electrons in both radiative and convective thermal transport leads to interest in electron density measurement. The present study deals with a measurement of electron density near the stagnation line of a two-dimensional shock-heated argon flow around a cylinder-plate (Fig. 1). The purpose of the work was to make a quantitative comparison between measured results obtained by optical interferometry and the predictions of equilibrium flow theory, using the Rankine-Hugoniot and Saha equations. A noble gas is desirable as the working fluid, since ionization can be studied without the complications of dissociation. In particular, argon was chosen because of its moderate ionization potential and relatively high molecular weight, which enabled significant ionization to be obtained behind the standing shock.

---

*) Numbers in brackets subsequently designate References collected at the end of this paper.

The technique of optical interferometry depends upon changes in index of refraction of the test gas, and has long been used to map densities in non-ionized flows. But Alpher and White [6] demonstrated that interferometry at optical wave lengths could be used to measure electron densities in a plasma. Since the refractivity of atoms is relatively insensitive to wave length, while the refractivity of electrons is highly dispersive, measurement of fringe shifts at two wave lengths enables the electron contribution to be separated. This yields a direct measurement of electron density, independent of the state of equilibrium of the plasma. Klein [7] applied this method to two-dimensional flow around a model in an electromagnetically-driven shock tube, but the flow entering the standing shock was highly non-uniform. Wong [8] has utilized this two wave length technique to study the relaxation zone behind the moving shock in argon. His work, using the same combustion driven tube as the present study, reinforces the conclusion drawn from Figs. 2 and 3 that flow entering the standing shock is quite uniform.

The present study is part of a long range program at Stanford dealing with the dynamics and properties of shock-heated plasmas. In particular, the present problem has direct application to ionization phenomena in the close environment of hypersonic vehicles, such as communications blackout.

II. EQUILIBRIUM FLOW THEORY

A. Introduction

In order to estimate the stagnation region electron density, it is necessary to calculate the state properties of argon at the stagnation line. Beginning with the state of the gas in the expansion chamber prior to the arrival of the incident shock wave (Fig. 1, region 1), the one-dimensional state calculations are made across the incident and standing shocks, assuming adiabatic flow and the attainment of local thermodynamic equilibrium after each shock. The equilibrium assumption is justified for region 2 by the work of Wong [8], as well as the interferograms in Figs. 2 and 3 of the present work. The computation is completed by assuming that the gas flows isentropically and incompressibly from the standing shock to the stagnation line.

B. Gas Properties Across Shock Waves

Properties across both shock waves are calculated using the Rankine-Hugoniot equations for a partially ionized, monatomic gas in conjunction with the Saha equation. The validity of the Saha equation for the equilibrium argon plasma has been demonstrated by Wong [8] and Cole [12]. Results of a computer program obtained by Wong were used to obtain the state of the gas in region 2. The equations used across the standing shock follow.

The degree of ionization, x, is defined by

$$x = \frac{N_e}{N_A + N_{A^+}} \quad ,$$

where N_A, N_{A^+} and N_e are number densities of atoms, ions, and electrons in any region of flow. The Saha equation, applied to the atom-ion-electron gas, is

$$x = \left[\frac{B_A(T) ph_P^3 \, e^{\chi/kT}}{2B_{A^+}(T)(2\pi\mu)^{3/2}(kT)^{5/2}} + 1 \right]^{-1/2} \quad ,$$

where p and T are the pressure and temperature, h_p is Planck's constant, χ is the ionization potential, and μ is the reduced mass of the ion-electron pair. In order to make use of the Saha equation, it is necessary to approximate B_A and B_{A^+}, the partition functions of the atom and ion. Since the neutral atom of argon has about 60 excited states near the ionization potential, the partition function is approximately

$$B_A(T) = 1 + 60e^{-\frac{162,500}{T}} ,$$

where $162,500^\circ K.$ is the ionization temperature. Since the temperatures involved are less than $15,000^\circ K.$, it is evident that the second term can be neglected. The argon ion has a ground state of multiplicity four, and a low level excited state of multiplicity two. Neglecting higher levels, the partition function of the ion is

$$B_{A^+}(T) = 4 + 2e^{-\frac{2060}{T}} .$$

Bond [9] estimates that neglect of these higher levels and the second ionization of the atom will not introduce appreciable error below $15,000^\circ K.$ Using these approximations, the Saha equation becomes

$$x = \left[\frac{ph_p^3}{(2\pi\mu)^{3/2}(kT)^{5/2}\, 4\left(2+e^{-\frac{2060}{T}}\right)} e^{\frac{182,100}{T}} + 1 \right]^{-1/2} .$$

The equation of state of an ionized monatomic gas in thermodynamic equilibrium is

$$p = (1+x)\,\rho RT = \rho \bar{R} T ,$$

where $\bar{R}$ is the average gas constant per unit mass of the mixture, and the masses of the ion and atom are considered equal.

The one-dimensional equations of conservation of mass, momentum, and energy for flow across a normal shock are unchanged by ionization:

$$\rho_2 v_2 = \rho_3 v_3$$

$$\rho_2 v_2^2 + p_2 = \rho_3 v_3^2 + p_3$$

$$\frac{1}{2} v_2^2 + h_2 = \frac{1}{2} v_3^2 + h_3 \quad .$$

The velocities (v) are given in the laboratory system, i.e. a system fixed with respect to the standing shock. These equations may be combined to obtain

$$h_3 - h_2 = \frac{1}{2}\left(\frac{1}{\rho_3} - \frac{1}{\rho_2}\right)\left(p_3 - p_2\right) \quad . \tag{II-1}$$

If excitation energy is neglected, the specific enthalpy is given by

$$h = e_t + e_i + \frac{p}{\rho} \quad ,$$

where e_t is the internal energy per unit mass due to translation, and e_i is the specific ionization energy. They are given by

$$e_t = \frac{3}{2}\overline{R}T = \frac{3}{2}\frac{R^*}{\overline{W}}T = \frac{3}{2}\frac{R^*}{W}(1+x)T = \frac{3}{2}R(1+x)T \quad ,$$

and

$$e_i = \frac{x(N_A + N_e)\chi}{\rho} = \frac{N_e k\theta}{\rho} = \frac{N_e k\theta}{m_a(N_e/x)} = xR\theta \quad ,$$

where R^* is the gas constant per mole, W is the atomic weight of argon, $\overline{W}$ is the average mixture molecular weight, θ is the ionization temperature, and m_A is the mass of the argon atom. Finally, the specific enthalpy is

$$h = \frac{5}{2}(1+x)RT + xR\theta \quad .$$

Substituting this in Eq. (II-1), the Rankine-Hugoniot equation becomes

$$\frac{\rho_3}{\rho_2} = \frac{4\,\frac{p_3}{p_2} + 1}{\frac{p_3}{p_2} + 4 - 2\left(\frac{x_3 - x_2}{1+x_2}\right)\frac{\theta}{T_2}} \quad . \tag{II-2}$$

A third equation, obtained by applying the equation of state on each side of the shock wave, is

$$\frac{T_3}{T_2} = \left(\frac{1+x_2}{1+x_3}\right)\frac{p_3}{p_2}\,\frac{\rho_2}{\rho_3} \quad . \tag{II-3}$$

A fourth independent relation is found by eliminating v_3 from the continuity and momentum equations to obtain

$$v_2^2 = \frac{p_2}{\rho_2} \cdot \frac{\rho_3}{\rho_2} \cdot \frac{(p_3/p_2) - 1}{(\rho_3/\rho_2) - 1} \quad .$$

The densities are eliminated from the preceding equation by substitution from Eq. (II-2) and the equation of state. The result is

$$v_2^2 = (1+x_2)RT_2\,\frac{\left(4\,\frac{p_3}{p_2} + 1\right)\left(\frac{p_3}{p_2} - 1\right)}{3\left(\frac{p_3}{p_2} - 1\right) + 2\left(\frac{x_3 - x_2}{1+x_2}\right)\frac{\theta}{T_2}} \quad . \tag{II-4}$$

To obtain this equation in terms of Mach number, the speed of sound in region 2, a_2, is required. For a monatomic, ionized gas, a_2 is expressed as

$$a_2 = \sqrt{\gamma\,\overline{R}T_2} = \sqrt{\frac{5}{3}\,R(1+x_2)T_2} \quad .$$

Dividing Eq. (II-4) by a_2^2, and solving for the pressure ratio p_3/p_2, the result is

$$\frac{p_3}{p_2} = \frac{1}{8}\left\{3 + 5M_2^2 + 5\left[(1-M_2^2)^2 + \frac{32}{15}\,\frac{(x_3 - x_2)}{(1+x_2)}\,\frac{\theta M_2^2}{T_2}\right]^{1/2}\right\} \quad ,$$

where M_2 is the Mach number entering the standing shock. This

equation, along with the Saha equation, and Eqs. (II-2) and (II-3), form a determinate system for the four unknowns p_3 , ρ_3 , T_3 and x_3 . The one-dimensional conservation equations used in this derivation are valid when applied to equilibrium regions on each side of a thin normal shock. Since the thickness of the non-equilibrium region in Fig. 3 is about half of the shock stand-off distance, the assumption of one-dimensional flow through the shock may be questionable.

C. Stagnation Line Gas Properties

If the flow from region 3 to the stagnation line is assumed adiabatic and non-heat conducting, then the total enthalpy is constant along any equilibrium streamline. In particular, along the central streamline, the enthalpy is given by

$$h_s = h_3 + \frac{1}{2} v_3^2 \quad .$$

The integrated one-dimensional conservation equations used across the shock are inappropriate as the flow becomes two-dimensional approaching the stagnation line. But Euler's equation along the central stream tube can be written as

$$vdv + \frac{dp}{\rho} = 0 \quad ,$$

where neglect of viscous stresses is justified by the relatively high densities, hence Reynolds numbers, involved. The assumptions of adiabatic, non-conducting, equilibrium, non-viscous flow imply the assumption of isentropic flow. Integrating the previous equation, we obtain

$$\int_3^s \rho v dv + \int_3^s dp = - \frac{\bar{\rho} v_3^2}{2} + p_s - p_3 = 0 \quad .$$

If the flow is also assumed to be incompressible, then $\bar{\rho}=\rho_3=$const. , and the result is simply Bernoulli's equation:

$$p_s = p_3 + \frac{1}{2} \rho_3 v_3^2 \quad .$$

The assumption of incompressible flow is hardly tenable for the hot, ionized gas, even at the low Mach number involved. But, since Rutowski [4] estimates the density change to be small, Bernoulli's equation will be used in these calculations.

With stagnation enthalpy and pressure known, the previously derived equations of specific enthalpy and state, and the Saha equation are applied at the stagnation point to solve for ρ_s , x_s , and T_s . These equations are

$$h_s = \frac{5}{2}(1+x_s)RT_s + x_s R\theta \quad ,$$

$$\rho_s = \frac{p_s}{(1+x_s)RT_s} \quad ,$$

and

$$x_s = \left[\frac{p_s h_p^3 \, e^{\frac{182,100}{T_s}}}{(2\pi\mu)^{3/2}(kT_s)^{5/2}\, 4(2+e^{-2060/T_s})} + 1 \right]^{-1/2} .$$

Results of the iterative solution were used to calculate N_{e_s} from the relation

$$N_{e_s} = \frac{\rho_s x_s}{m_A} .$$

III. APPLICATION OF INTERFEROMETRY TO ELECTRON DENSITY MEASUREMENT

A. The Mach-Zehnder Interferometer

A schematic of the interferometer is shown in Fig. 9. Monochromatic light from the source is collimated before entering the half-silvered beam splitter S_1. Here the light is split into two beams, which travel via the fully silvered mirrors M_1 or M_2 to be recombined at the second beam splitter S_2. The light is focused by the lens L_2, and the camera is placed at the focal plane of the test section.

If the mirrors were all perfectly parallel, and the optical path lengths of the two beams exactly equal, one would expect reinforcement of the in-phase beams, resulting in a uniformly bright image at the camera. Now, if one of the mirrors is rotated slightly, a uniformly varying difference in optical path is introduced, resulting in alternating reinforcement and destruction, i.e., a fringe pattern. If now a plasma is formed in the test section, the index of refraction, and hence the optical path length, of one beam is changed, resulting in a fringe shift given by

$$S = \frac{\Delta\, nL}{\lambda} = \frac{\Delta\,(n-1)L}{\lambda} \quad ,$$

where $\Delta\,(n-1)$ is the change in refractivity, L is the test section width, and λ is the monochromatic observing wave length. The compensating chamber is introduced to compensate for the windows of the test section of the shock tube.

Since the primary quantity desired is electron density at the stagnation line, the problem is to relate the observed fringe shift (from ahead of the standing shock, 2, to the stagnation line, s) to the change in electron density. Conditions behind the moving shock, 2 , are taken from calculations by Wong [8], which were verified experimentally by him.

B. Development of Fringe Shift Equations

In order to relate the observed fringe shifts to electron density, the refractivities of the neutrals, ions, and electrons must be related to thermodynamic quantities.

The refractivity of the neutrals is obtained from the polarizability of the atom, α_A, by the equation

$$n_A - 1 = 2\pi \alpha_A N_A = \frac{2\pi \alpha_A}{m_A} (N_A m_A) = K_\lambda m_A N_A \quad ,$$

where $K_\lambda = (2\pi \alpha_A / m_A)$ is the Gladstone-Dale constant, which varies only slightly with wavelength. The atom number density is related to the degree of ionization by

$$N_A = \frac{\rho}{m_A} (1-x) \quad .$$

Therefore, the change in refractivity of the neutrals between any two regions is

$$\Delta (n_A - 1) = K_\lambda \Delta [\rho(1-x)] \quad .$$

Similarly, the ion refractivity is given by

$$n_{A^+} - 1 = 2\pi \alpha_{A^+} N_{A^+} = \frac{2\pi \alpha_{A^+}}{\alpha_A} \cdot \frac{1}{m_A} \cdot \alpha_A m_A N_{A^+} = K_\lambda \frac{\alpha_{A^+}}{\alpha_A} m_A N_{A^+} \quad .$$

The number density of the ions is

$$N_{A^+} = N_e = \frac{\rho x}{m_A} \quad .$$

The change in refractivity of the ions is

$$\Delta (n_{A^+} - 1) = K_\lambda \frac{\alpha_{A^+}}{\alpha_A} \Delta (\rho x) \quad .$$

The refractivity of the electrons is given by Wong [8] to be

$$(n_e-1) = -\frac{1}{2}\frac{\omega_P^2}{\omega^2} \quad ,$$

where ω_P, the plasma frequency, is given by

$$\omega_P^2 = \frac{4\pi q^2 N_e}{m_e} = \frac{4\pi q^2}{m_e m_A}(\rho x) \quad ,$$

ω is the observing light frequency, and where the assumption has been made that the electron-atom collision frequency is much less than the observing frequency. This assumption is valid for conditions of the present study. The change in refractivity due to electrons is

$$\Delta(n_e-1) = \frac{-q^2\lambda^2}{2m_e m_A \pi c^2}\Delta(\rho x) = -6.77 \times 10^8 \lambda^2 \Delta(\rho x) \quad ,$$

where λ is in centimeters, and $\Delta(\rho x)$ signifies the difference in the product of density and degree of ionization between any two regions.

Assuming that the refractivity changes for the various particles are independent, the total change in refractivity is

$$\Delta(n-1) = \Delta(n_A-1) + \Delta(n_{A^+} - 1) + \Delta(n_e-1) \quad .$$

Recalling that the total fringe shift across, for example, the standing shock is given by

$$S = \frac{L}{\lambda}\Delta(n-1) \quad ,$$

this fringe shift is expressed in terms of thermodynamic quantities by

$$S = L\left\{\frac{K_\lambda}{\lambda}\left[\rho_3(1-x_3)-\rho_2(1-x_2)+\frac{\alpha_{A^+}}{\alpha_A}(\rho_3 x_3-\rho_2 x_2)\right] -6.77 \times 10^8 \lambda(\rho_3 x_3-\rho_2 x_2)\right\} \qquad \text{(III-1)}$$

The ratio of polarizabilities of the argon ion and atom is taken as

$$\frac{\alpha_{A^+}}{\alpha_A} = 0.67 \quad ,$$

and the test section width for the present experiment was L=5.0 cm. Inserting these values and combining terms, the total fringe shift for $\lambda = 4500$ A is

$$S = 1.78 \times 10^4[\rho_3-\rho_2-8.86(\rho_3 x_3 - \rho_2 x_2)] \quad , \qquad \text{(III-2)}$$

where $K_{4500} = .1592$ cm^3/gm has been used. Similarly, for $\lambda'=4030$ A , $K_{4030} = .1609$ cm^3/gm , and the fringe shift is

$$S' = 1.993 \times 10^4[\rho_3-\rho_2-7.13(\rho_3 x_3 - \rho_2 x_2)] \quad . \qquad \text{(III-3)}$$

Combining the last two equations, the electron density in region 3 of the argon plasma is

$$N_{e_3} = N_{e_2} + 4.33 \times 10^{17}(S' - 1.1275) \quad , \qquad \text{(III-4)}$$

where $\lambda = 4500$ A , $\lambda' = 4030$ A , and S and S' are the measured fringe shifts at these wave lengths. With N_{e_3} now determined, either of the fringe shift equations, (III-2) or (III-3), can be used to solve for ρ_3 . Choosing the equation for $\lambda = 4500$ A , the result is

$$\rho_3 = \rho_2 + 5.63 \times 10^{-5} S + 5.86 \times 10^{-22}\left(N_{e_3} - N_{e_2}\right) \quad .$$

The degree of ionization can now be determined from

$$x_3 = \frac{N_{e_3} m_A}{\rho_3} \quad .$$

The last three equations are sufficient to determine electron density and degree of ionization at any point in the plasma from observed fringe

shifts between a known region and the region of interest. The fringe shift equations (III-2) and (III-3) may be used to predict fringe shifts from calculated plasma conditions, as in Fig. 4.

IV. DESCRIPTION OF EXPERIMENT

The experiment was performed using the Stanford aerophysics laboratory shock tube. Figure 8 is a schematic of the experimental arrangement. The 25 foot long driven section is constructed of extruded aluminum, with a two inch square inside cross section. The combustion driver uses a stoichiometric mixture of hydrogen and oxygen diluted with helium, which is ignited by a battery of spark plugs. The driver and driven sections are separated by a scribed aluminum diaphragm. Pumping of the driven section, to about 10^{-5} mm. Hg before filling, is accomplished through a station at each end of the section. The test section, located 20 feet from the diaphragm, supports the two-dimensional cylinder-plate model. A pair of optical windows permits viewing of flow about the model, and three barium titanate piezo-electric transducers just upstream of the model are used to measure the incident shock speed. The dump tank at the downstream end is separated from the driven section by a thin aluminum diaphragm which breaks on arrival of the incident shock.

The Mach-Zehnder interferometer (Fig. 9), located at the test section, is on loan through the courtesy of Lockheed Missiles and Space Company. The light source was obtained by discharging 16 kilovolts from a 7.5 microfarad capacitor across magnesium electrodes spaced about 1/4 inch apart. Although no direct measurement of the spark duration was made, oscilloscope pick-up of the capacitor "ringing" indicated that the spark was probably near maximum intensity during the entire exposure time of five microseconds. A blast shutter and pinhole were originally placed at the focal point of the light source in an attempt to reduce film exposure by plasma radiation. However, Fig. 10 shows that, even at relatively low Mach number, radiation reaching the film was intense enough to wash out completely the fringes through the 5890A filter.

Since it had become evident that the mechanical blast shutter was not fast enough for this application, a Kerr cell was obtained, again through the courtesy of Lockheed. This electronic shutter, manufactured by the Kappa Scientific Corporation of Sierra Madre, California, was

equipped with a pulse-forming network that permitted a very reproducable shutter-open time of five microseconds. For the present steady flow application, this exposure time proved satisfactory. Unfortunately for this application, it was designed for use in the ultraviolet, with acetronitrile as the working fluid. The Kerr cell was triggered to open for five microseconds during peak spark intensity, and the shutter-open period was always between 12 and 17 microseconds after passage of the incident shock by the model.

The flow field was split by interference filters passing 4500 and 5890 angstroms located just ahead of the Polaroid camera. Simultaneous measurements of near stagnation-line fringe shifts through the two filters were sufficient to determine the electron density. However, variation in intensity of the dark fringes passed by the 5890A filter (see Figs. 2,3) indicated the presence of a harmonic. Further, comparison of observed fringe shifts with Eqs. (III-2) and (III-3) showed that the "5890" fringes actually corresponded to a wave length lower than 4500A . Examination of a spectrum obtained by Wong through this second order 5890A filter, also using a magnesium spark source, showed a third order pass band at 4030A . It was concluded that peaking of the ultraviolet Kerr cell at about 4000A , as well as the low intensity of the magnesium spectrum at 5890A , resulted in a fringe pattern dominated by $\lambda' = 4030$A . The existence of harmonics in the fringe pictures indicates that the presence of some 5890A might cause a small increase in effective wave length above the value of $\lambda' = 4030$A used in the calculations.

An attempt was made to obtain total stagnation line heat transfer data using a platinum thick-film calorimeter, as described by Rutowski [4]. Initial efforts indicated that this phase of the program would require more effort than originally anticipated. Because of practical limitations of time, it was decided to concentrate remaining efforts on the interferometric studies.

V. DISCUSSION OF RESULTS

Usable fringe shift data were obtained for both $\lambda = 4500$ A and $\lambda' = 4030$ A on four runs. These were made at incident shock Mach numbers of 11.45, 11.8, 12.0, and 12.8. The lowest Mach number was obtained with an initial pressure (p_1) of 10 mm. Hg. , while the others corresponded to p_1=5 mm. All tests were made in argon, with the 1/2 inch diameter cylinder-plate model installed in the test section. Graphs of fringe shift, density ratio, electron density, and degree of ionization (Figs. 4,5,6 and 7) compare predicted and measured quantities in region 3, just downstream of the standing shock. Figure 7 also shows measured stagnation line degree of ionization and the corresponding prediction of equilibrium theory.

Attainment of equilibrium in region 2, the flow entering the standing shock, was found by Wong [8] to occur about six microseconds after the incident shock (lab time) for the lowest Mach number of the present study, while the prediction of Petschek and Byron [10] is somewhat less. Since the present interferograms were taken between 12 and 17 microseconds after the incident shock, it is reasonable that the flow entering the standing shock was in equilibrium. The interferograms in Figs. 2 and 3 show relatively straight fringes in region 2, supporting the conclusion of equilibrium there. The compensating effects of incident shock wave attenuation and radiative cooling on the flow in region 2 were discussed by Rutowski and Bershader [5]. Although the magnitude of these effects has not been determined, their effect probably was minimized by taking all the interferograms at the same time relative to the incident shock. Total available test time was estimated to be about 100 microseconds for the fastest run.

The interferograms at the two lower Mach numbers (Fig. 2a) show a sharp upward (positive) fringe shift across the standing shock due to change in refractivity of the heavy particles [Eq. (III-1)]. These shifts were found to correspond not to the predictions of equilibrium theory [Eq. (III-2)], but to the estimate obtained by assuming degree of ionization frozen at the value in region 2, and equilibration of the

translational modes only. Predicted quantities based on these assumptions were obtained from the perfect gas shock tables of Keenan and Kaye [11], for $\gamma=5/3$, and the results are compared with measured values of fringe shift, density ratio, and degree of ionization in Figs. 4, 5, and 7. Since measurements at the stagnation line showed only a small increase in degree of ionization from that in region 3 (Fig. 7), the flow field from the standing shock to the stagnation line is concluded to be definitely out of chemical equilibrium, and in fact nearly frozen. Measured values of electron density in region 3, which differed only moderately from those measured at the stagnation line, are shown in Fig. 6 to be much less than the corresponding equilibrium predictions.

The interferograms at the two higher Mach numbers (Fig. 2b) show a radical change in the flow field. The shock stand-off distance is reduced by more than a factor of two. The initial upward fringe shift again roughly corresponds to the frozen prediction, with the larger shift at the lower wave length, as would be expected from Eq. (III-1), for the heavy particles. But a large shift in the opposite direction, i.e. due to electron production [Eq. (III-1)] is also observed. Since this shift is proportional to wave length, it is greater for $\lambda = 4500$ A.

The flow appears to approach local equilibrium at the line of maximum downward fringe shift, located about half way from the shock to the stagnation line. Since the fringe shift due to electrons from region 2 to 3 is somewhat less than predicted for equilibrium (Fig.4), the measured values of electron density obtained from Eq. (III-4) only approach the equilibrium estimate. It is possible that application of the one-dimensional conservation equations across a shock extending half way to the stagnation line is invalid, which could explain the lower measured equilibrium densities. A better theory would make use of a one-dimensional analysis across the frozen portion of the shock, and calculate the approach to equilibrium by a two-dimensional theory utilizing a rate equation. However, the change in the fringe pattern (Fig. 3) perpendicular to the flow direction is small near the centerline of flow, indicating that the flow across the shock is nearly one-dimensional

in the region of interest. The flow from region 3 to the stagnation line causes an upward shifting of fringes, which for these conditions can only be caused by ion-electron recombination [Eq. (III-2)]. This effect, which of course is not predicted by the adiabatic equilibrium analysis, is illustrated by a small decrease in degree of ionization from region 3 to the stagnation line at M_s=12.0 , and a larger decrease at the higher Mach number (Fig. 7). Although the Kerr cell effectively reduces the interferogram exposure from plasma radiation, other pictures, using only the blast shutter, show the existence of strong radiation in this Mach number range. It appears to be concentrated in the region behind the bow shock, and is probably largely due to radiative recombination. It is concluded that the flow at the higher Mach numbers does approach equilibrium momentarily, but immediately begins cooling due to radiative losses. Radiative recombination could also explain the lower than expected equilibrium electron densities measured in region 3. The sharp change in stand-off distance over a very small Mach number range may be related to the attainment of equilibrium at the higher speeds. Table II summarizes these observations on the flow interferograms.

Although no rigorous theory has yet been developed for convective stagnation region heat transfer in a partially ionized monatomic gas, the Fay-Riddell correlation equation [1] has been applied to this situation by Reilly [3] and Rutowski and Bershader [5]. Predicted heat transfer rates based on this equation depend on the value chosen for the Lewis number, but do not vary markedly from the ideal gas prediction based on the same equation. Both Reilly and Rutowski and Bershader found substantial agreement of measured convective heat transfer rates with estimates based on the equation of Fay and Riddell. The present study suggests that the flow field ahead of Reilly's model was probably nearly frozen, since his study used a much smaller model and lower initial pressures than the present work, and involved Mach numbers of 12 or less. A similar comparison of the present study with the experiments of Rutowski and Bershader, involving Mach numbers greater than 11.7, initial pressures of 10 mm. Hg. , and a larger model, indicates that equilibrium was probably attained in the stagnation region during

their work. These considerations suggest that the state of equilibrium of the shock-heated argon plasma does not critically affect stagnation region convective heat transfer. This result is not entirely unexpected, since convective heat transfer is basically a boundary layer phenomenon. In the first approximation, it should be relatively insensitive to shock layer rate processes, particularly for the relatively high densities involved in the present study (Table I).

Rutowski and Bershader suggest a radiative heat transfer model based on an extension of Kramers classical theory for free-free (bremsstrahlung) radiation to include radiative recombination into the upper bound states. Assuming thermodynamic equilibrium they estimate radiative heat transfer rate to be proportional to the square of electron density. Use of predicted electron densities in the present case would have resulted in grossly overestimated radiative heat transfer for the frozen tests, but a much smaller error at the higher Mach numbers, where equilibrium was attained.

The following factors were considered as possible contributors to error of the experimental measurements:

1. Error in determination of Mach number by the pressure transducer-oscilloscope system is estimated to be about 1%.
2. Actual initial temperatures varied from $T_1=297^{\circ}K$ to $T_1=304^{\circ}K$. Since all theoretical calculations were based on $T_1=300^{\circ}K$, a small scatter in the (uncorrected) measured values would be expected.
3. The work of Wong [8] indicates that the presence of impurities could cause a decrease in the relaxation time. However, this effect was predicted primarily for very low initial electron densities, where atom-atom collisions are predominant. Since all regions of interest in the present study involve relatively high electron densities, and the tube pressure before filling was about 10^{-5} mm. Hg. for all runs, the effect of impurities is not considered significant.

4. Fringe shifts could be read to an accuracy of about one-tenth of a fringe. An error in this measurement would introduce only a small discrepancy between predicted and measured fringe shifts at a single known wave length (Fig. 4, λ=4500A). Therefore, it is considered that qualitative observations from Fig. 4, i.e. separation of frozen and equilibrium regimes, are valid.

5. However, the measured values of electron density, degree of ionization, and density ratio, which were all obtained from measured fringe shifts at two different wave lengths, are subject to more serious error. The proximity of the two observing wave lengths (λ=4500A, and λ'=4030A) results in sensitivity of Eq. (III-4) to small errors in reading the fringe shift, especially at lower Mach numbers where the shift due to electrons is small. It will be recalled that original plans had called for using λ'=5890A as the second wave length, which would have resulted in considerably better accuracy. There is an additional uncertainty in the actual value of the lower wave length (λ'=4030A + ~100A , - 0A) . This is derived from the possibility that presence of traces of 5890A might result in an "effective" $\lambda' > 4030A$. Elimination of all 5890A radiation by procuring a suitable additional filter was precluded by time considerations. Use of a higher "effective wave length vice λ'=4030A in the calculations would have resulted in a fairly uniform increase in the measured electron density for all runs. The estimated uncertainty in measured electron density due to these considerations is included in Fig. 6. It should be noted that this interferometric method is capable of considerably greater accuracy than the present work obtained. However, the agreement of density ratios (Fig. 5) obtained by the two-wave length technique with the appropriate theory (frozen or equilibrium) corresponds to the conclusions drawn from the more accurate single-wave length fringe shift predictions (Fig. 4).

VI. CONCLUSIONS

1. Flow entering the standing shock was in equilibrium during each test.

2. Stagnation region equilibrium was not attained during the two lower Mach number tests. The degree of ionization remained essentially frozen at its value entering the standing shock.

3. During the higher speed tests, local thermodynamic equilibrium was achieved ahead of the stagnation point. The thickness of the relaxation region was about half of the shock stand-off distance. The degree of ionization after relaxation was less than the equilibrium prediction, and actually decreased from the end of the relaxation zone to the stagnation line. The lower than expected degree of ionization in both regions 3 and s is attributed to radiative recombination.

4. Since radiative heat transfer has been related to the square of electron density, the present work indicates somewhat less radiative heat transfer than predicted by equilibrium theory. But the observed recombination provides some justification for considering radiative recombination a primary component of stagnation region thermal transport.

REFERENCES

1. Fay, J. A., and F. R. Riddell, Jour. Aero. Sci., 25, 73, 1958.

2. Rose, P. H., and W. I. Stark, Jour. Aero. Sci., 25, 86, 1958.

3. Reilly, J. P., Stagnation Point Heating in Ionized Monatomic Gases, Fluid Mechanics Laboratory Publication No. 64-1, Massachusetts Institute of Technology, 1964.

4. Rutowski, R. W., Stagnation Point Heat Transfer in a Partially Ionized Gas, Proceedings of the 1959 Heat Transfer and Fluid Mechanics Institute, Stanford University Press, Stanford, California, 1959.

5. Rutowski, R. W., and D. Bershader, Phys. of Fluids, 7, 568, 1964.

6. Alpher, R. A., and D. R. White, Phys. of Fluids, 2, 162, 1959.

7. Klein, A. F., A Survey of Optical Interferometry as Applied to Plasma Diagnostics, Aerospace Corporation 63-377, 1963.

8. Wong, H., Interferometric Study of Thermal Equilibration of a Shock Heated Plasma, Ph.D. Thesis, Stanford University, California, April 1964.

9. Bond, J. W., Phys. Rev. 105, 1683, 1957.

10. Petschek, H. E., and S. Byron, Ann. Phys., 1, 270, 1957.

11. Keenan, J. H., and J. Kaye, Gas Tables, Wiley and Sons, 1948.

12. Cole, W., unpublished Engineer Thesis, Stanford University, 1964.

TABLE I

CALCULATED STATE PROPERTIES OF EQUILIBRIUM ARGON

Initial Conditions: p_1 = 5mm.Hg. , = 1.07×10^{-5} gm/cm^3

$T_1 = 300^{\circ}K$

State Property	Shock Mach Number, M_s		
	11	12	13
p_2 (mm)	795.5	972	1168
ρ_2 (gm/cm^3)	4.94×10^{-5}	5.54×10^{-5}	6.15×10^{-5}
T_2 ($^{\circ}K$)	10,100	10,880	11,500
x_2	.0204	.0305	.0602
N_{e_2} (cm^{-3})	1.52×10^{16}	3.22×10^{16}	5.59×10^{16}
p_3 (mm)	2534	3642	4990
ρ_3 (gm/cm^3)	12.5×10^{-5}	16.1×10^{-5}	20.2×10^{-5}
T_3 ($^{\circ}K$)	12,065	12,930	13,820
x_3	.0705	.1100	.152
N_{e_3} (cm^{-3})	1.33×10^{17}	2.72×10^{17}	4.62×10^{17}
p_s (mm)	3090	4340	5448
ρ_s (gm/cm^3)	14.8×10^{-5}	18.8×10^{-5}	21.3×10^{-5}
T_s ($^{\circ}K$)	12,410	13,240	14,080
x_s	.080	.118	.162
N_{e_s} (cm^{-3})	1.79×10^{17}	3.34×10^{17}	5.20×10^{17}

TABLE II

SUMMARY OF TEST OBSERVATIONS

Shock Mach Number (M_s)	p_1 (min.)	Shock Stand-Off Distance δ/D	Relaxation Distance	Radiation	Stagnation Line Electron Density N_{e_s} (cM^{-3})
11.45	10	.620	$> \delta$ near frozen in shock layer.	Significant in shock layer.	Much lower than equilibrium prediction.
11.8	5	.690	↓	↓	↓
12.0	5	.332	$\approx \delta/2$ local equilibrium attained.	Brilliant in shock layer; fringes indicate some recombination.	Lower than equilibrium prediction.
12.8	5	.286	$< \delta/2$ local equilibrium attained.	Brilliant in shock layer; fringes indicate significant recombination.	↓

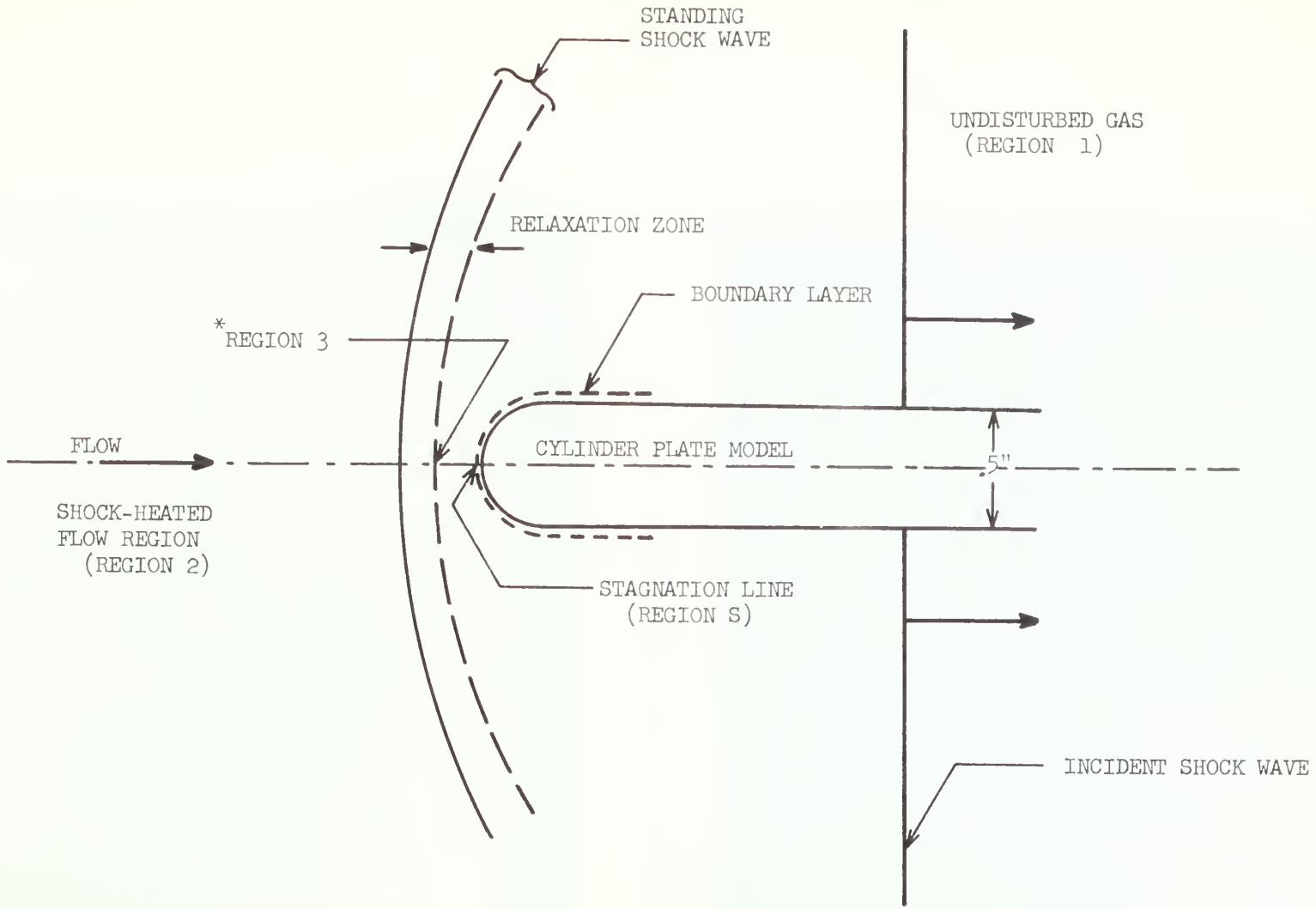

*Note: For the "frozen" tests, the standing shock is defined by the initial frozen fringe shift only.

Fig. 1. Schematic Diagram of Shock-Generated Flow.

λ'=4030A

λ=4500A

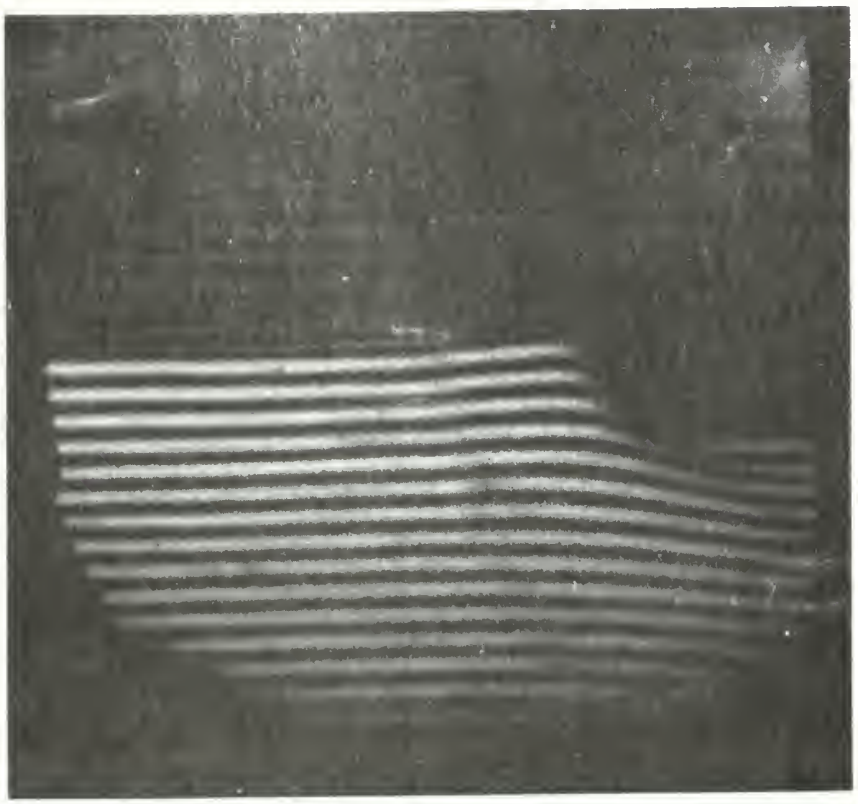

Fig. 2a. Flow Interferogram (M_s=11.45) .

λ'=4030A

λ=4500A

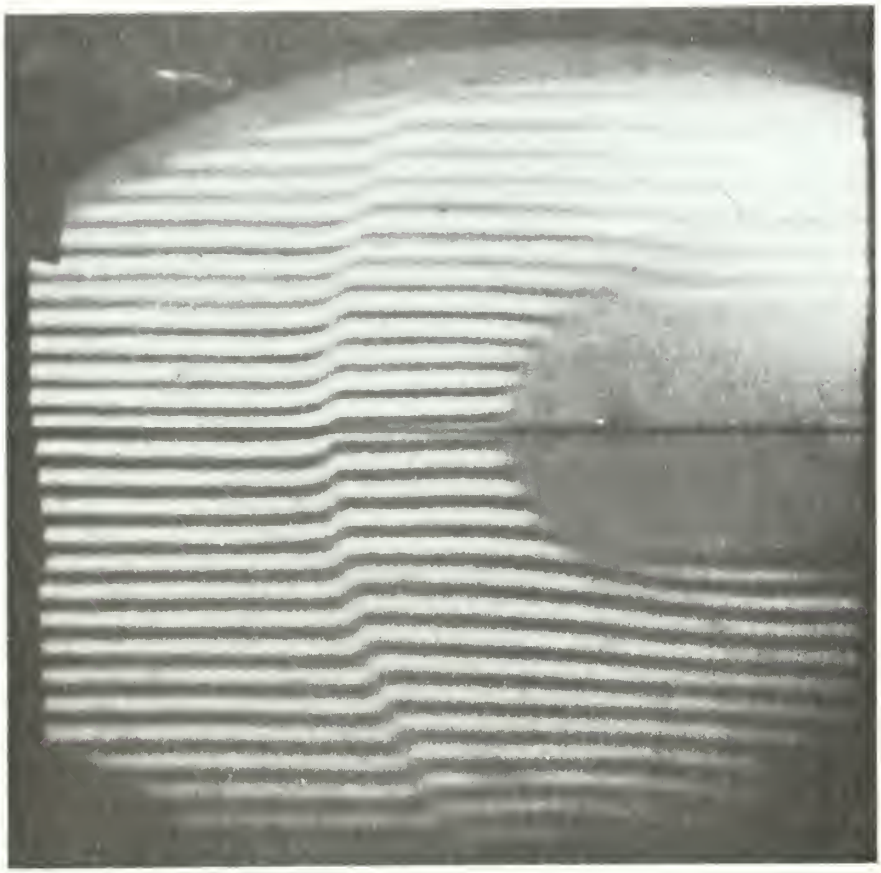

Fig. 2b. Flow Interferogram (M_s=11.8) .

λ'=4030A

λ=4500A

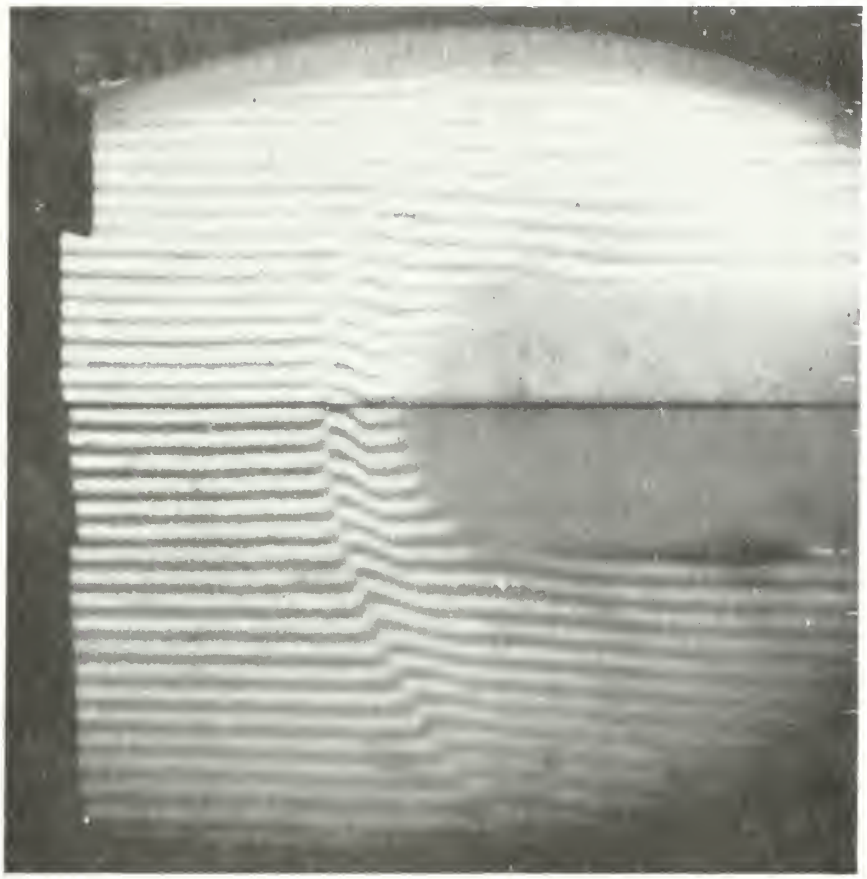

Fig. 3a. Flow Interferogram (M_s=12.0) .

λ'=4030A

λ=4500A

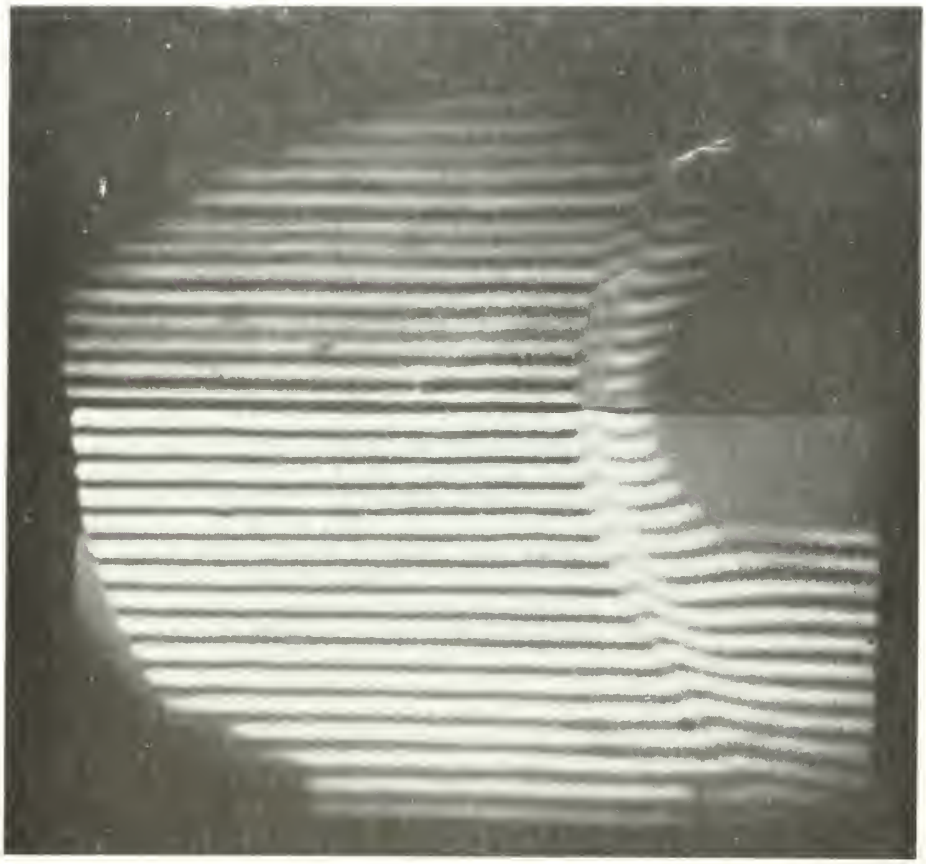

Fig. 3b. Flow Interferogram (M_s=12.8) .

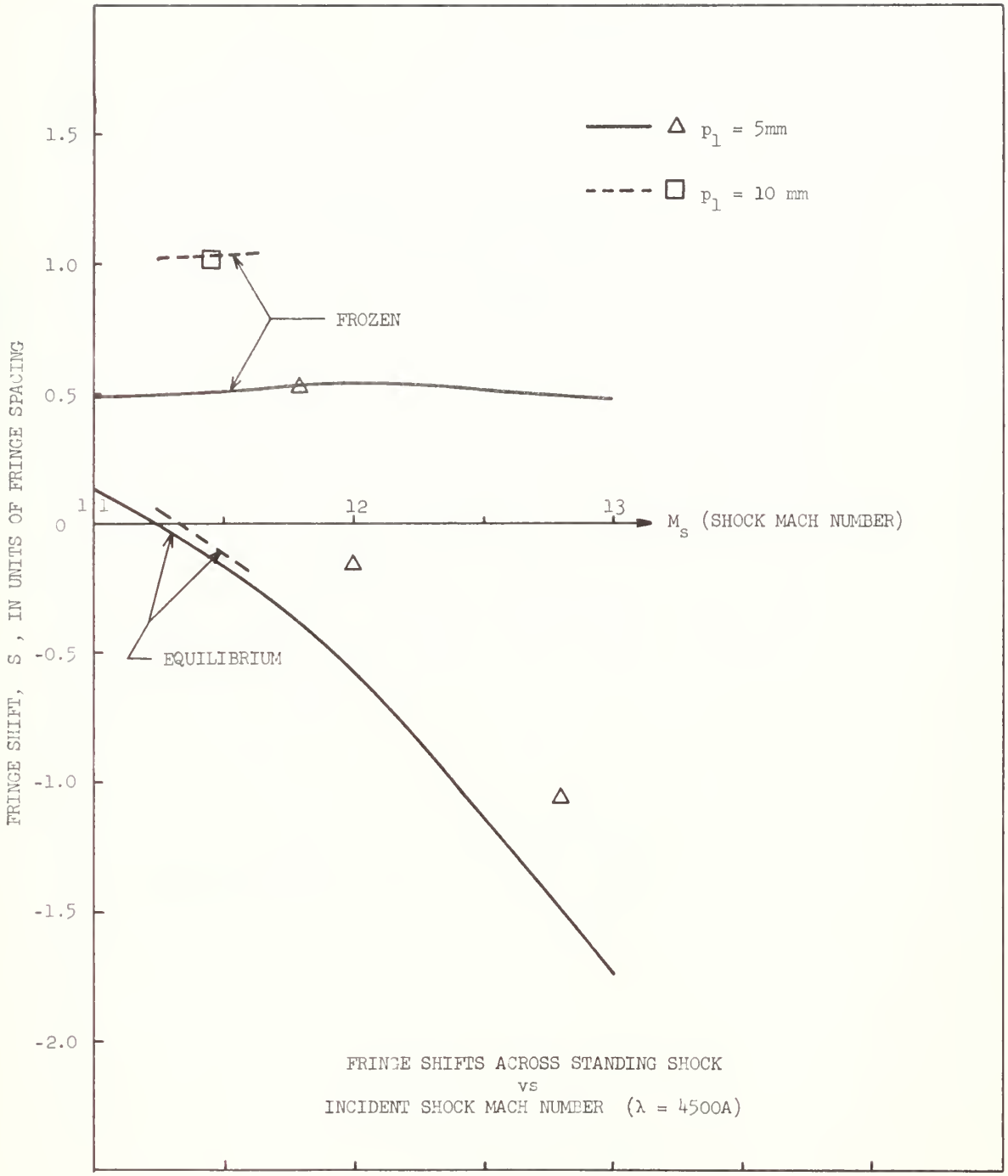

Fig. 4. Fringe Shifts.

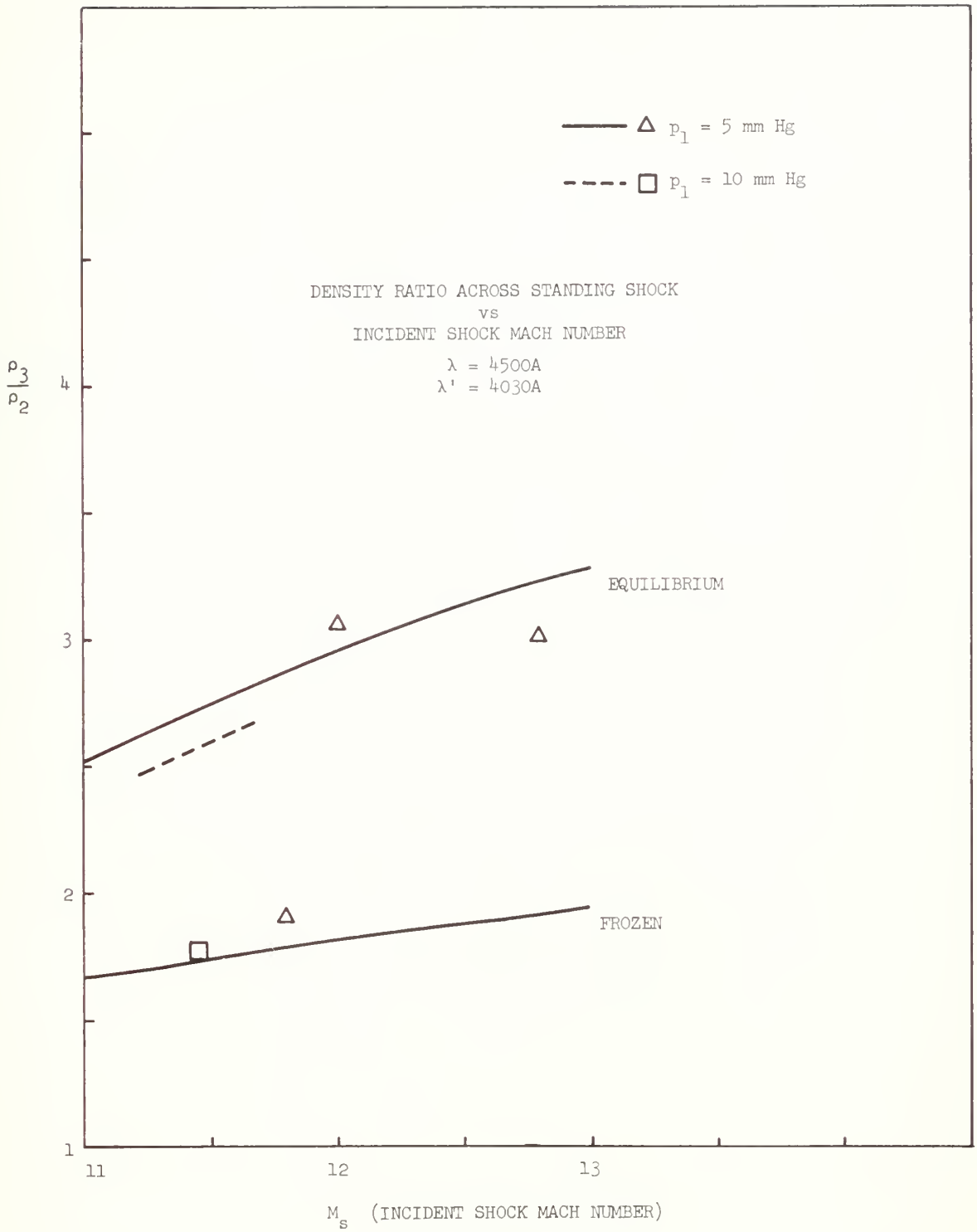

Fig. 5. Density Ratio.

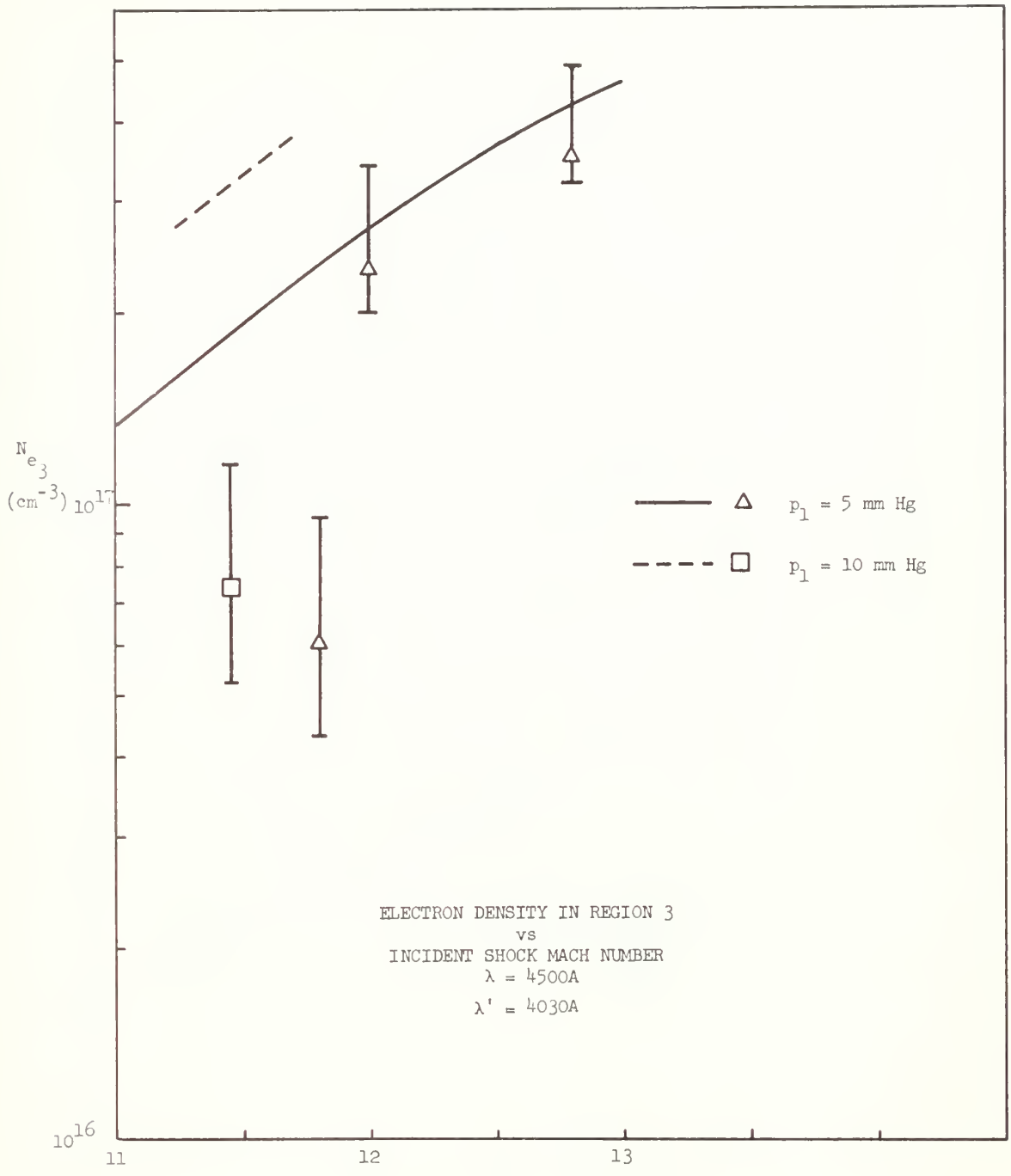

Fig. 6. Electron Density.

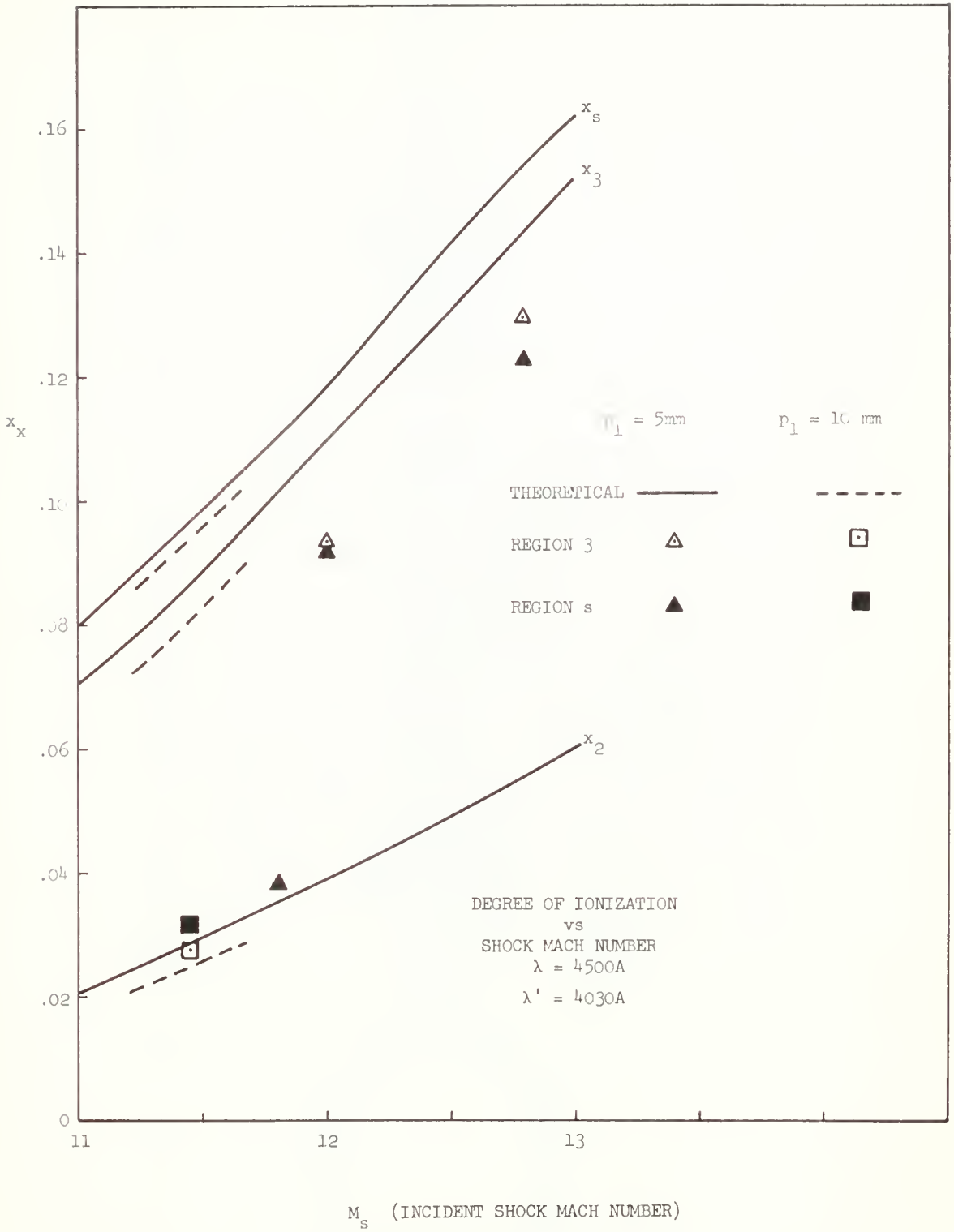

Fig. 7. Degree of Ionization.

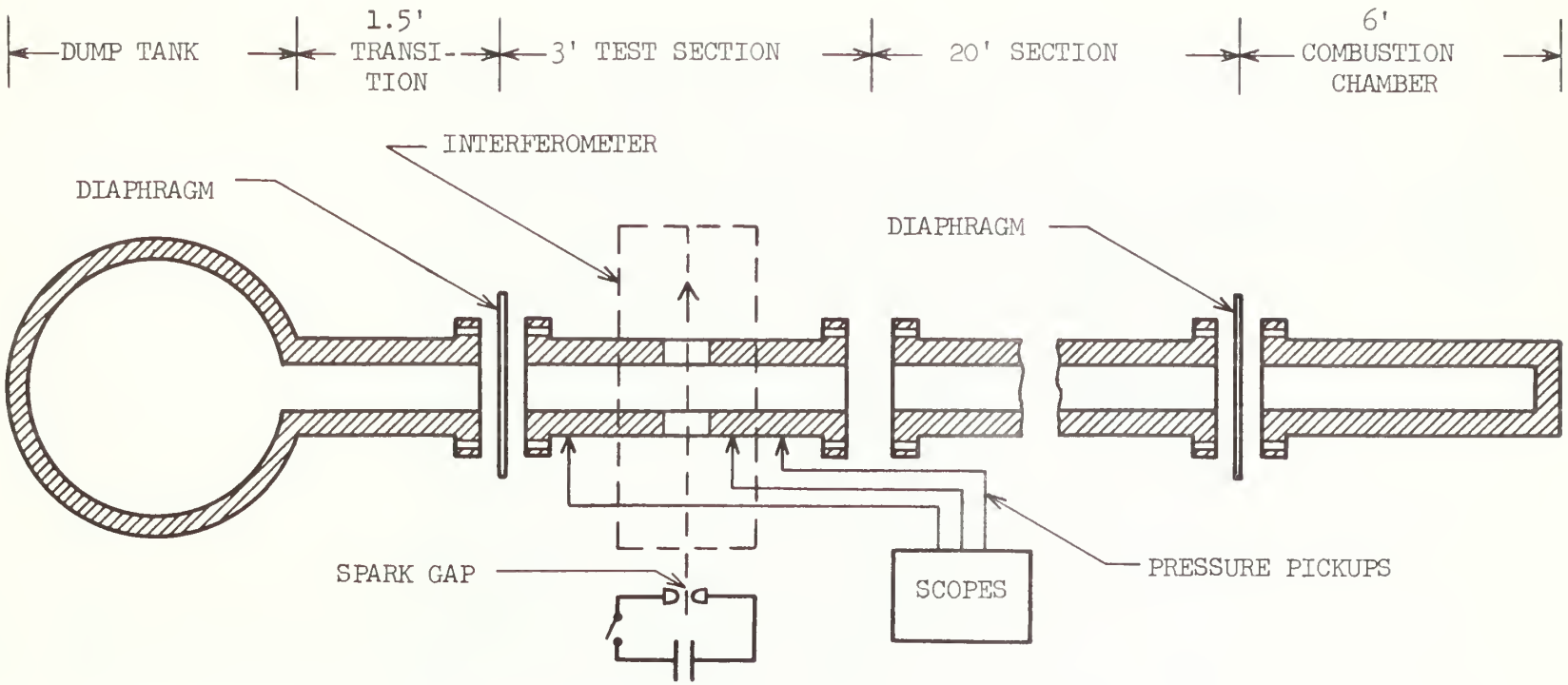

Fig. 8. Stanford Shock Tube.

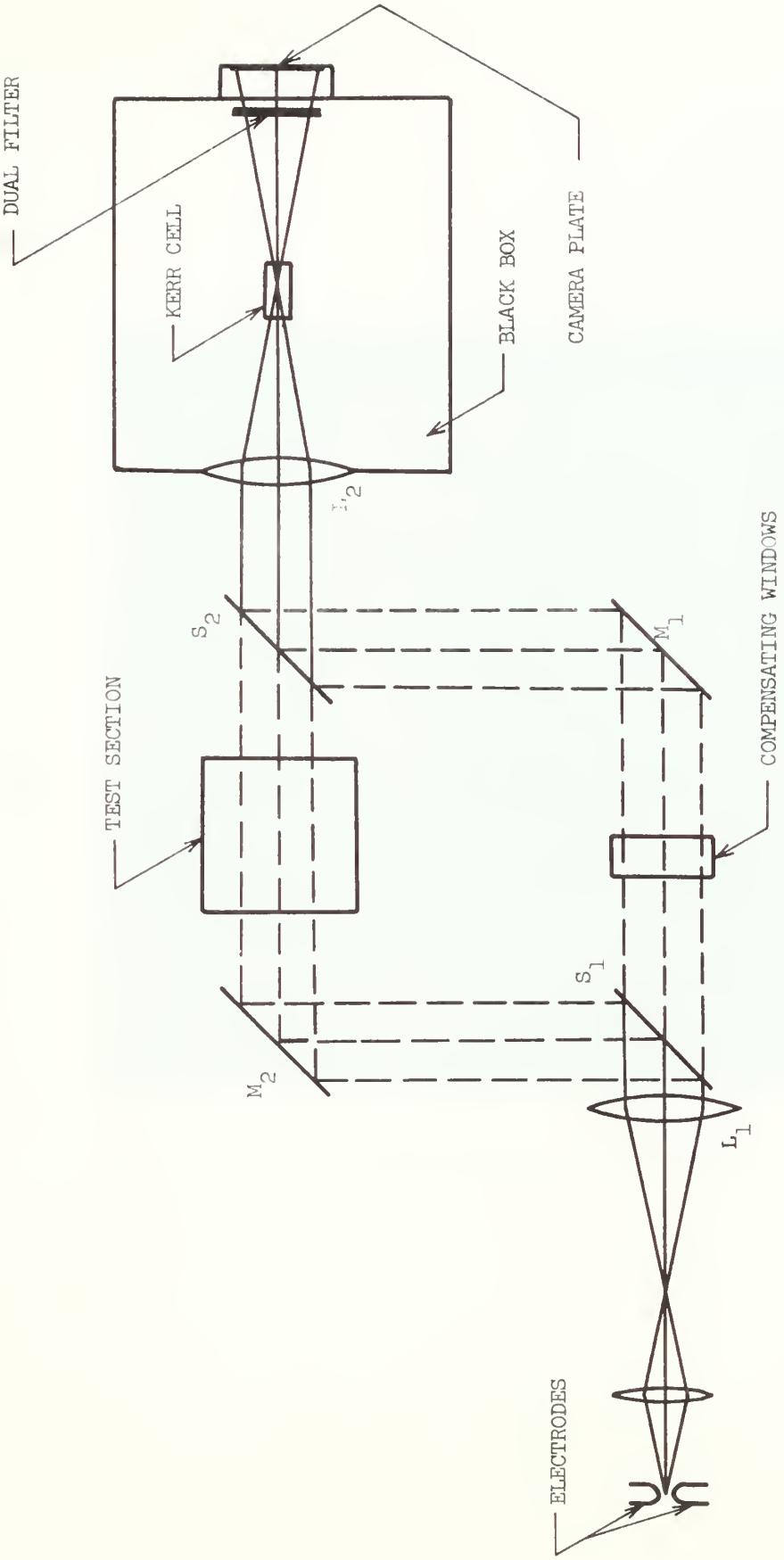

Fig. 9. Schematic of Optics.

λ=4500A

Fig. 10. Blast Shutter Interferogram.